CEAS COUNCIL OF EUROPEAN AEROSPACE SOCIETIES

Aerospace Europe
6th CEAS Conference

Time-domain aeroelastic model for compound helicopter propeller-wing configuration

Zi Wang
PhD Student at the University of Nottingham
Department of Mechanical, Materials and Manufacturing Engineering,
University of Nottingham, University Park, Nottingham, UK, NG7 2RD
Zi.Wang@nottingham.ac.uk

Alessandro Anobile
Research Fellow at the University of Nottingham

Atanas A. Popov
Professor at the University of Nottingham

ABSTRACT

A simplified numerical model for time-domain aeroelastic analysis of a wing structure in a propeller-wing configuration is described in the paper. A linear beam model with deformable elastic axis under torsional deformation and out-of-plane bending is considered to simulate a wing structure with tip mounted propeller, relying on efficient, analytical formulations. The complete aeroelastic system of equations is solved using Galerkin's approach, and numerically integrated by the Newmark-beta method. The computational tool developed is able to predict the wing aeroelastic transient behaviour and the wing-propeller interaction effects in the time domain. The purpose of such a tool is to provide accurate enough predictions of the system aeroelastic response to be included in structural optimisation and control synthesis procedures. A complete analysis on the solver used and an aeroelastic analysis of a Eurocopter X3-like compound helicopter wing/propeller configuration are demonstrated.

KEYWORDS: *Aeroelasticity, Rotorcraft, Compound helicopter, Wing-propeller interaction*

NOMENCLATURE

a – Dimensionless parameter, measuring distance of shear centre from mid-chord
b – Half chord length
c_x , ζ_x – Damping coefficient
EI, GJ – Bending and torsional stiffness
$F_{\text{gen}}, M_{\text{gen}}$ – Generalized force and moment
I_α – Mass moment of inertia per unit span
J_x, Y_x – Bessel functions
k_p – Propeller encounter frequency
L – Wing semi-span length
L_x, l_x – Lift and its dimensionless expression $(L_x b/mU_\infty^2)$
m, μ – Mass per unit span, dimensionless mass parameter $(m/\pi\rho b^2)$
$\mathbf{M}, \mathbf{C}, \mathbf{K}$ – Mass, damping and stiffness matrices
M_x, m_x – Moment and its dimensionless value $(M_x b^2/I_\alpha\, U_\infty^2)$
r_α – Dimensionless radius of gyration $\sqrt{I_\alpha/mb^2}$
χ_α – Dimensionless static unbalance from shear centre $(\text{static unbalance}/mb)$
$S(k_p)$ – Sears' function
$\boldsymbol{u}, \boldsymbol{F}$ – Displacement and loading vectors
U_∞, V_x – Advancing speed and its dimensionless value $(U_\infty/b\omega_\alpha)$
U_p – Propeller axial velocity
w_G – Total gust velocity field
ξ, α – Dimensionless bending and torsional displacements
ω_x – Natural frequencies
ω_p – Propeller frequency
$\overline{\omega}$ – Frequency ratio (ω_h/ω_α)
ρ – Air density
τ, τ_0 – Dimensionless time
ϕ, ψ – Wagner's and Küssner's functions

0 – Initial conditions
h, α – Bending and torsional direction
a – Wagner's model related loadings
g – Küssner's model related loadings
s – Sears' model related loadings
i, j - Mode number integer

1 INTRODUCTION

In the past ten years, the concept of compound helicopter has emerged in rotorcraft designs. Having the capability to take-off and land vertically using a main rotor like a helicopter, compound helicopters are also equipped with additional systems for improving performance in fast forward flight. An implementation of such configuration has been demonstrated by the Eurocopter (Airbus Helicopters) X3. Besides the conventional helicopter fuselage, two short wings are added with tip-mounted propellers. Inheriting most characteristics from conventional helicopters, its propeller-wing configuration allows to achieve much higher cruising speeds, going beyond typical limitations of conventional helicopters. However, the still open issue of high level of vibration resulting from fluid-structure interaction is exacerbated in the case of compound helicopters, with even more critical effects on fatigue life of structures, maintenance costs, on-board instrumental efficiency and comfort. Therefore, being able to model and predict the complex aeroelastic behaviour associated with the wing-propeller system becomes extremely important to achieve an optimised design of such aircraft configuration.

The aim of this paper is to investigate the effects of the aeroelastic interaction between wing and propeller in a compound helicopter using simple models and numerically efficient methods. The ultimate goal is to develop an accurate and reliable tool able to provide aeroelastic predictions without the numerical effort needed for more accurate analyses. Such a tool will be well suited for structural optimisation or control synthesis procedures, where a high number of simulations are needed, or in the early stages of design to have preliminary predictions of structural vibration, when information about the structural components is limited.

For achieving this aim, a simplified model is introduced to simulate the time-domain aeroelastic response of the fixed wing. Aerodynamics and structural dynamics of the wing are characterised separately and coupled in the equations of motion. The fixed-wing structure is modelled as a cantilever beam with deformable elastic axis under torsional deformation and out-of-plane bending. The propeller attachment requires a relatively rigid wing which makes it reasonable to remain under the linear model assumption of small displacements. The unsteady aerodynamic loads are considered and derived by analytical sectional models based on Wagner's function [1], where three-dimensional effects are taken into account as inflow corrections quantified as output of an external aerodynamic simulation. The influence of propeller on the wing is also modelled through periodic wake inflow in vertical and axial components using Sears' [2] and Küssner's [3] gust models. Related to the propeller location, the inflow properties vary along the wing span. Therefore, in this propeller-wing configuration, a simplified sectional model with uniform conditions is not sufficient in modelling the entire wing. Thus, to enable properties variation along the wing span, a continuous beam model gives a better representation for the wing structure in such configuration.

On similar topics, numerical studies were carried out in the past to model the unsteady response of elastic wings under vertical gusts relying on simplified sectional model. Sears and Sparks [4] studied the effect of a sharp-edged gust on an elastic in bending but torsional rigid wing using Jones' approximation [5, 6] of Wagner's function. As performed by Jones for the Wagner's function, a similar exponential expression was proposed for the Küssner's function by Sears and Sparks for its simplicity [4]. In a more recent work, the plunging motion of a typical sectional model under sharp edged gust was further analysed for its flutter boundaries and studied under several flutter related conditions by Kargarnovin and Mamandi [7]. Extending the sectional model to two degrees of freedom, namely bending and torsion, aeroelastic analysis under sharp edged gust was carried out by Shams et al. using a recursive approximation for Wagner's function [8]. Additional studies were carried out by Marzocca et al. that examined the aeroelastic instability and response of 2D aerofoil under arbitrary gust loadings using Wagner's and Küssner's unsteady aerodynamic models [9]. Similar sectional models were also used in a slightly different field, for prediction of vibratory loads and aeroacoustic effects due to an extremely three dimensional phenomenon, such as blade-vortex interaction, in helicopter rotor blades. Two-dimensional Theodorsen's theory was applied to predict aerodynamic loads in an aeroelastic tool including inflow corrections from a 3D, free wake BEM aerodynamic simulation [10]. In the aeroacoustic work, pressure distribution on the rotor blades was calculated using the Küssner-Schwartz theory [11] with external inflow corrections, again from BEM simulations [12].

Using Galerkin's method and pre-assumed mode shape functions, the governing equations of motion are written in a matrix form. The complete aeroelastic system of equations is then numerically solved using the Newmark-beta method [13]. A complete analysis on the solver used and further validations against similar problems in the past literature are presented.

2 MATHEMATICAL MODEL

In order to describe the aeroelastic analysis tool developed, a structural model and an aerodynamic model are analysed separately. For the structural model, a linear cantilever Euler-Bernoulli beam is used to represent the wing chosen, where the linear assumption remains valid due to the small displacements experienced by the structure. Concerning the aerodynamic model, the unsteady aerodynamics behaviour is captured through analytical theories of 2D aerofoil under incompressible flow. In the following paragraphs, these models are described along with their integration to form the mathematical model for simulation of the aeroelastic response of a compound helicopter propeller-wing configuration.

2.1 Structural Model

The structural dynamics of a cantilever linear beam is used to simulate the vibration behaviour of the wing structure on the compound helicopter. The reference system used in the following description is the one shown in Figure 1. Having x-axis going through the elastic axis of the wing, torsional and out-of-plane bending elastic degrees of freedom are considered.

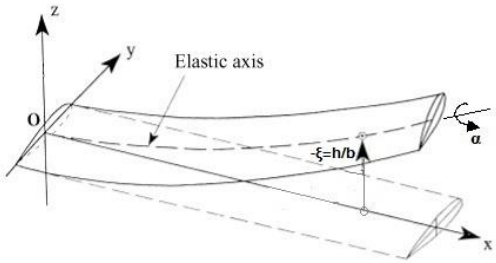

Figure 1: Beam based model with flapping and torsion

The normalised structural equations in dimensionless time-domain form can be formulated as

$$\begin{aligned} &\ddot{\xi} + \chi_\alpha \ddot{\alpha} + \frac{c_h b}{m U_\infty}\dot{\xi} + \frac{EIb^2}{m U_\infty^2}\xi'''' = l_h(x,\tau) \\ &\ddot{\alpha} + \frac{\chi_\alpha}{r_\alpha^2}\ddot{\xi} + \frac{c_\alpha b}{I_\alpha U_\infty}\dot{\alpha} - \frac{GJb^2}{I_\alpha U_\infty^2}\alpha'' = m_\alpha(x,\tau) \end{aligned} \quad (1)$$

In Eq.1, ξ, α are the dimensionless bending and torsional displacements, m is the mass per unit span, I_α being the mass moment of inertia per unit length, U_∞ is advancing speed of the aircraft, b is the half chord length, χ_α is the dimensionless static unbalance at the shear centre, r_α is the dimensionless radius of gyration , c_h, c_α being the damping coefficient, EI, GJ are the bending and torsional stiffness respectively and l_h, m_α being dimensionless loadings in its corresponding coordinate. Note that $\dot{\xi}\ \ddot{\xi}\ \dot{\alpha}$ and $\ddot{\alpha}$ are time differentials with respect to the dimensionless time, whereas ξ' and α' are length differentials with respect to the x-coordinate.

Using modal analysis techniques, bending and torsional displacements can be rewritten as product of time-dependent functions and mode shape functions.

$$\begin{aligned} &\xi = \textstyle\sum_{j=1}^{\infty} \theta_j(x) q_j(t) \\ &\alpha = \textstyle\sum_{j=1}^{\infty} \eta_j(x) z_j(t) \end{aligned} \quad \text{where} \quad \begin{aligned} &\theta_j(x) = \cosh(\lambda_j x) - \cos(\lambda_j x) - \sigma_j\,[\sinh(\lambda_j x) - \sin(\lambda_j x)] \\ &\eta_j(x) = \sqrt{2}\sin(2j-1)\pi x/2L \end{aligned} \quad (2)$$

In Eq.2, mode shape coefficients $\lambda_j L$ and σ_j are defined as below.

Table 1: Mode shape function coefficients for bending

Mode No.	1st	2nd	3rd	4th	5th
$\lambda_j L$	1.8750	4.6941	7.8548	10.9955	14.1372
σ_j	0.7341	1.0185	0.9992	1.0000	0.9999

Loadings in bending and torsional coordinate (l_h, m_α) are made up of generalised beam loadings and aerodynamic loadings. In addition to the aerodynamic loads, only the concentrated propeller weight at wingtip ($F_{\text{gen}} = \frac{b}{mU_\infty^2} \times \text{propeller weight}$) is taken into account in this case, neglecting effects of forward thrust and rotational moment. Also at this stage, the wing dynamics is not coupled with the propeller dynamics, assuming only the tip-weight on the cantilever beam and the aerodynamic interaction as effects of the propeller presence. Concerning the aerodynamic loadings, they are obtained using the models described below.

2.2 Aerodynamic Model

The aerodynamic loadings can be split in different contributions, including: 1) constant advancing flow along wing span, 2) additional advancing flow at propeller covered area produced by thrust generation, 3) an "equivalent step–gust" $w_0(x,\tau)$ applied along the wing span to model the wing pre-twist angle, and 4) sinusoidal vertical inflow produced by propeller presence. They can be characterised analytically relying on sectional aerodynamic theories, which consider the increment of circulation and apparent mass to formulate unsteady aerodynamic loadings. In the theory of oscillating aerofoils, circulation is determined by the downwash velocity at the 3/4 chord point from the leading edge and can be formulated by considering the convolution superposition integral. On the other hand, acceleration of apparent mass forms the non-circulatory lift. In the case studied, applications of three aerodynamic models are presented, namely Wagner's model, Küssner's model and Sears' model, to characterise aerodynamic loadings from in-plane (y) and out-of-plane (z) velocity components.

A fixed-wing with built-in angle in forward flight is only subjected to a constant advancing speed along the span and a vertical components (simulated as "equivalent step–gust") due to the pre-twist angle and angle of attack. In the application considered, the presence of the propeller in front of the wing, as source of forward thrust, affects the wing performance by its wake slipstream. As illustrated in Figure 2, the inflow coming from the propeller has two main characteristic velocity components, one being axial and the other being a vertical component. At this level, the third component, horizontal along the wing span, is neglected. The inflow considered can be evaluated with different simulation techniques and then included as inflow correction in the sectional models used to estimate the wing aerodynamic loads. With this correction, also loads due to the wing-propeller interaction can be taken into account.

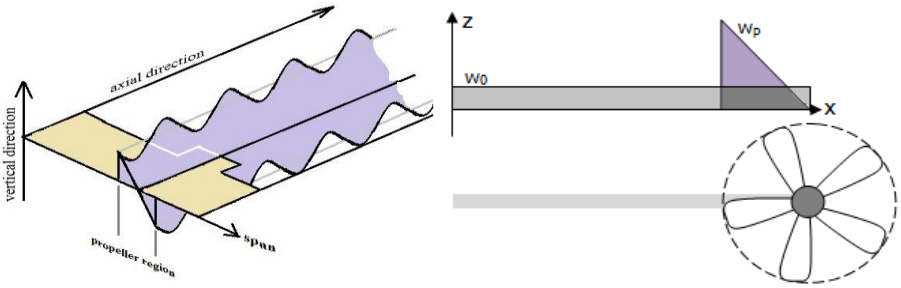

Figure 2: Propeller-axial (yellow) and vertical (purple) velocity contributions

An accurate prediction of the propeller downstream inflow affecting the wing is beyond the scope of this work. In order to present the capabilities of the analysis tool developed and illustrate its application, a simplified inflow distribution is considered. In the propeller-axial direction, an increase of incident flow velocity is implemented as a step change across the propeller covered length (see the yellow area in Figure 2). The propeller axial effect and the constant span-wise advancing flow due to the forward flight form a distributed advancing speed profile, which can be taken into account by Wagner's model. Wagner's model considers the angle of attack (AoA) changes to formulate aerodynamic lift component as for the wing

$$l_a(x,\tau) = -\frac{2}{\mu}\phi(\tau)\left(\alpha_0 + \dot{\xi} + \left(\frac{1}{2}-a\right)\dot{\alpha_0}\right) - \frac{2}{\mu}\int_0^\tau \phi(\tau-\tau_0)\left(\dot{\alpha} + \ddot{\xi} + \left(\frac{1}{2}-a\right)\ddot{\alpha}\right)d\tau_0 - \frac{1}{\mu}\left(\ddot{\xi} - a\ddot{\alpha} + \dot{\alpha}\right)$$
$$m_a(x,\tau) = \frac{2}{r_\alpha^2\mu}\left(\frac{1}{2}+a\right)\phi(\tau)\left(\alpha_0 + \dot{\xi} + \left(\frac{1}{2}-a\right)\dot{\alpha_0}\right) - \frac{2}{r_\alpha^2\mu}\left(\frac{1}{2}+a\right)\int_0^\tau \phi(\tau-\tau_0)\left(\dot{\alpha} + \ddot{\xi} + \left(\frac{1}{2}-a\right)\ddot{\alpha}\right)d\tau_0 +$$
$$\frac{a}{r_\alpha^2\mu}\left(\ddot{\xi} - a\ddot{\alpha}\right) - \frac{1}{r_\alpha^2\mu}\left(\frac{1}{2}-a\right)\dot{\alpha} - \frac{1}{8}\frac{1}{r_\alpha^2\mu}\ddot{\alpha} \qquad (3)$$

Eq.3 gives the Wagner's component for lift l_a and moment m_a in dimensionless form with $\mu = m/\pi\rho b^2$ being the mass parameter. In the model presented, Wagner's function $\phi(\tau)$ is defined as Jones' approximation [5, 6]. This exponential approximation is chosen for its simplicity of the recursive algorithm used. However, other forms of Wagner's function approximation can also be found in References [11, 14, 15].

At the same time, as the propeller slipstream passes the wing, it gives a vertical induced inflow on the wing, similar to a localised gust. A linear gust velocity profile is assumed along the span with propeller mounted at wing tip, as shown by the purple area in Figure 2. Due to the harmonic nature of the slipstream, a sinusoidal gust is also assumed with 10% of the vertical gust effect as its variation amplitude. Thus, the total vertical localised gust $w_G(x,\tau)$ in the wing sections affected by the propeller field includes the pre-twist angle equivalent to gust with velocity $w_0(x,\tau)$, the vertical propeller inflow contribution $w_p(x,\tau)$, and the sinusoidal gust variation at frequency $k_p = \omega_p b/U_p$ with magnitude of $w_i(x)$. It can be defined as

$$\begin{aligned} &\text{when } \tau<0, \quad w_G(x,\tau) = 0 \\ &\text{when } \tau>=0, w_G(x,\tau) = w_0(x,\tau) + w_p(x,\tau) + |w_i(x)|\sin(k_p\tau - k_p(1+a)). \end{aligned} \tag{4}$$

In the rest of the wing span, only $w_0(x,\tau)$ is present.

For a complete analysis, the Küssner's model is used. Küssner's function enables the modelling of aerofoil going through arbitrary gust field as successive step changes, and formulates lift generated on the wing

$$l_g(x,\tau) = -\frac{2}{\mu}\int_0^\tau w_G(\tau_0)\frac{d\psi(\tau-\tau_0)}{d\tau}\,d\tau_0\,;\; m_g(x,\tau) = \frac{2}{r_\alpha^2\mu}\left(\frac{1}{2}+a\right)\int_0^\tau w_G(\tau_0)\frac{d\psi(\tau-\tau_0)}{d\tau}\,d\tau_0 \tag{5}$$

In Eq. 5, Küssner's function $\psi(\tau)$ is defined as approximation by Sears and Sparks [4]. Other form of Küssner's function can be found in References [14, 15].

A final model presented is the Sears' one, which can be more efficient than Küssner's model if only steady-state analyses are performed. Sears' model provides the steady-state loads generated when an aerofoil is travelling through sinusoidal gust filed. In this special case, sinusoidal terms are excluded from Eq.5 in Küssner's model related calculations, instead, separate loading terms by Sears' model representing steady-state airloads are included.

For a sinusoidal gust field with amplitude of $|w_i|$, frequency of ω_p and advancing speed of U_p, an equivalent frequency-domain expression can be defined using Sear's function $S(k_p)$. The expressions of the lift, l_s, and moment, m_s, generated are:

$$l_s(x,\tau) = -\frac{2}{\mu}\frac{|w_i|}{U_p}S(k_p)\,e^{\sqrt{-1}k_p\tau};\; m_s(x,\tau) = \frac{2}{r_\alpha^2\mu}\left(\frac{1}{2}+a\right)\frac{|w_i|}{U_p}S(k_p)\,e^{\sqrt{-1}k_p\tau} \tag{6}$$

In Eq.6, the Sears' function is dependent on encounter frequency $\boldsymbol{k_p}$ and defined in terms of Bessel functions as can be found in References [11, 14, 15].

2.3 Aeroelastic Modelling

By combining the structural dynamics equations and the aerodynamic loadings, the governing aeroelastic equations can be obtained. To solve this continuous system, Galerkin's method is used with the assumed mode shape functions defined in Eq.2. Multiplying the flapping equation by $\int_0^L \theta_i dx$ and the torsional equation by $\int_0^L \eta_i dx$ the following expressions are obtained:

$$\sum_{j=1}^{\infty}\left[\int_0^L \theta_i\theta_j dx\,\ddot{q}_j + \chi_\alpha\int_0^L \theta_i\eta_j dx\,\ddot{z}_j + 2\zeta_h\frac{\overline{\omega_j}}{V_j}\int_0^L \theta_i\theta_j dx\,\dot{q}_j + \left(\frac{\overline{\omega_j}}{V_j}\right)^2\int_0^L \theta_i\theta_j dx\,q_j\right] = \int_0^L \theta_i\left(l_a + l_g + F_{\text{gen}}\right)dx$$

$$\sum_{j=1}^{\infty}\left[\int_0^L \eta_i\eta_j\,dx\ddot{z}_j + \frac{\chi_\alpha}{r_\alpha^2}\int_0^L \eta_i\theta_j dx\,\ddot{q}_j + 2\zeta_\alpha\frac{1}{V_j}\int_0^L \eta_i\eta_j dx\,\dot{z}_j + \left(\frac{1}{V_j}\right)^2\int_0^L \eta_i\eta_j dx\,z_j\right] = \int_0^L \eta_i\left(m_a + m_g + M_{\text{gen}}\right)dx$$

A general matrix form of the governing equation can be written as

$$\mathbf{M}\ddot{\boldsymbol{u}} + \mathbf{C}\dot{\boldsymbol{u}} + \mathbf{K}\boldsymbol{u} = \boldsymbol{F} \tag{7}$$

Where $\mathbf{M}, \mathbf{C}, \mathbf{K}$ represent the mass, damping, stiffness matrices, with $\boldsymbol{u}, \boldsymbol{F}$ being displacement and loading vectors respectively. The governing equations of motions are solved by Newmark-beta method. Based on convergence studies performed, the dimensionless time step is chosen to be 1/8 of the smallest period involved in the analysis. Moreover, five modes of bending and one torsional mode

have been chosen after performing additional convergence analyses aimed at determine the best trade-off between accuracy involved and the computational effort needed.

3 RESULTS AND DISCUSSION

3.1 Model validation

The aeroelastic model presented has been validated against results from Shams et al. [16] as illustrated in Figure 3. In Shams' paper, the nonlinear aeroelastic response of a continuous beam system was studied using a similar numerical approach. The linear model presented in Section 2.3 is able to reproduce a similar pre-flutter behaviour to the Shams' nonlinear model. As shown in Figure 3, a comparison between aeroelastic behaviours from these two models is obtained.
In Shams et al. paper [16], a nonlinear beam model was initially disturbed in the plunging direction for 0.2m under its pre-flutter condition considering three coupled modes (two bending and one torsion). Plunging and pitching displacements at the tip were measured and showed as function of time. In comparison with the results provided by the presented linear model, a perfect agreement is shown in the plunging displacement as shown in Figure 3 (on the left side). For the pitching behaviour in Figure 3 (on the right side), frequency and damping are well reproduced for the same condition but not the maximum amplitude of the oscillations. However, as the motions were initially excited by a plunging displacement, bending and torsional motion coupling due to nonlinearity terms present in Shams' model contributed to the differences observed.

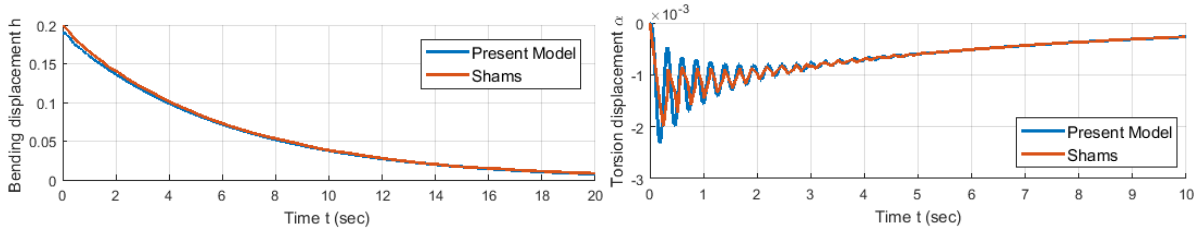

Figure 3: Results compared with Sham's results from [16]

3.2 Case study with compound helicopter parameters

For the study presented in the following sections, a wing-propeller system similar to Eurocopter X3 is considered and the main specifications are listed in Table 2.

Table 2: Propeller-wing configuration details

Wing specification		**Surrounding air properties**	
Mass per span length	22.3040 kg/m	Air density	1.225 kg/m^3
Moment of inertia per span length	0.2908 kg/m	Advancing speed	120 m/s
Bending stiffness (EI)	3.2146e+5 Nm^2	**Propeller inputs properties**	
Torsional stiffness (GJ)	4.1276e+5 Nm^2	Propeller diameter	2 m
Chord length	0.6 m	Propeller mass	50 kg
Semi-wing span	2.5 m	Propeller location	Tip mounted
Shear & gravity centre offset	0 m		
Shear centre and mid-chord offset	0 m		
Pretwist angle	2°		

Based on the structural parameters given, the structural natural frequencies can be calculated using predefined mode shape coefficients. As shown in Table 3, natural frequencies up to 8 lowest modes are presented in bending and torsional direction. The aeroelastic results presented are based on simulations involving five bending and one torsional modes.

Table 3: Natural frequencies of bending and torsional modes

Bending & Torsional Natural Frequencies (Hz)			
1st Bending Mode	10.75	4th Bending Mode	369.61
2nd Bending Mode	67.36	5th Bending Mode	610.99
3rd Bending Mode	188.61	1st Torsional Mode	119.14

Concerning the propeller inflow modelling, an additional axial flow velocity of 8 m/s is added in the wing area affected by the propeller presence. In the vertical direction, a linear gust distribution, like the one illustrated in Figure 2, with maximum velocity of 7m/s, is applied on the propeller covered area with sinusoidal variation at a frequency of 145.6Hz (blade passage frequency), with 10% of the vertical gust effect as its variation amplitude.

3.3 Case Study Results

In this section, results related to the wing response in the presence of propeller-wing interaction are shown. The case study parameters are presented in Section 3.2. The wing is assumed to start from unloaded initial condition and to be excited by the propeller stream, already in regime condition. This situation is not realistic during the aircraft flight but it is considered to show the capability of the tool developed in modelling transient responses of the system with changing the propeller regime.

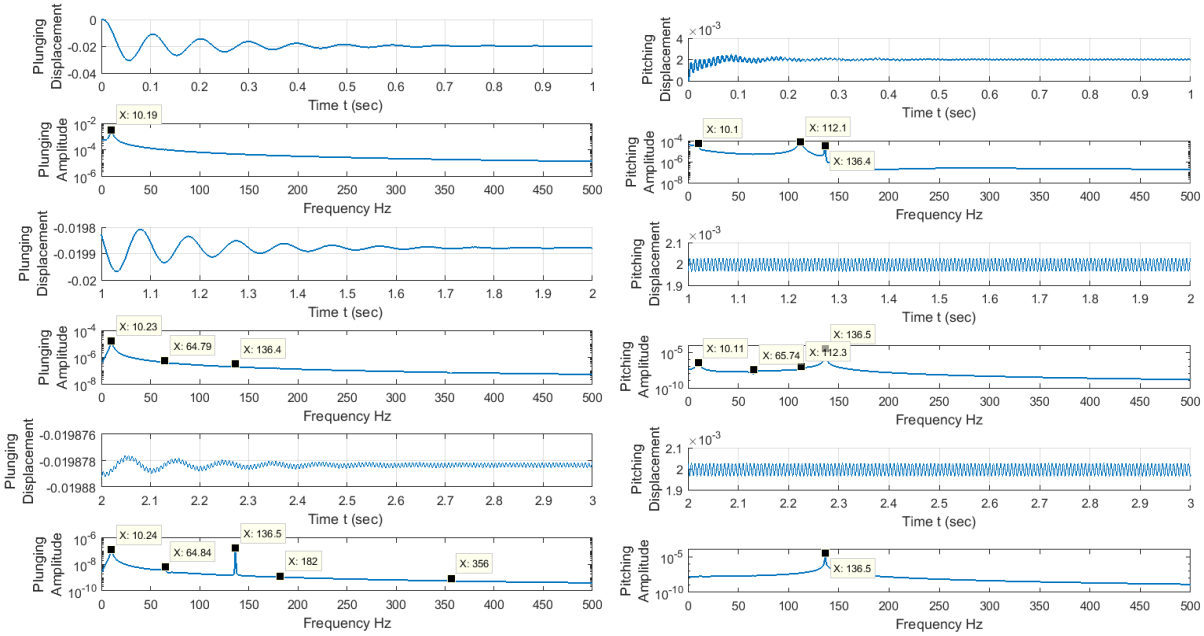

Figure 4: Aeroelastic transient response of a wing in propeller-wing configuration

In Figure 4, the transient wing response is shown from time t=0s to t=3s. Both time-domain and frequency-domain responses are shown, alternated in the different rows for every second of response. The response in terms of plunging motion of the wing section located at 75% of the span is shown in the left-hand side column, while the response in terms of pitching motion of the same section is shown on the right-hand side column.

As shown in the Figure 4, the propeller-wing system experiences a transient phase and reaches its steady state around t=3 seconds. During the transient phase, the first modes of bending and torsion are governing the main wing behaviour before the rising of the sinusoidal oscillations due to the interaction with the propeller stream. For plunging behaviour, during 1-3 seconds, as the first mode weakens, several other structural frequencies can be seen, and the propeller frequency starts to grow in relative contribution. On the other hand, the torsional behaviour showed similar pattern. Finally, the propeller inflow effect took over into the steady-state wing response, after the transient behaviour is completely damped.

The steady-state response, both time- and frequency-domain, of the aeroelastic system is shown in Figure 5. Following the transient phase, the propeller effect now governs the steady-state oscillations. Similar behaviour can be found in both bending and torsional motions.

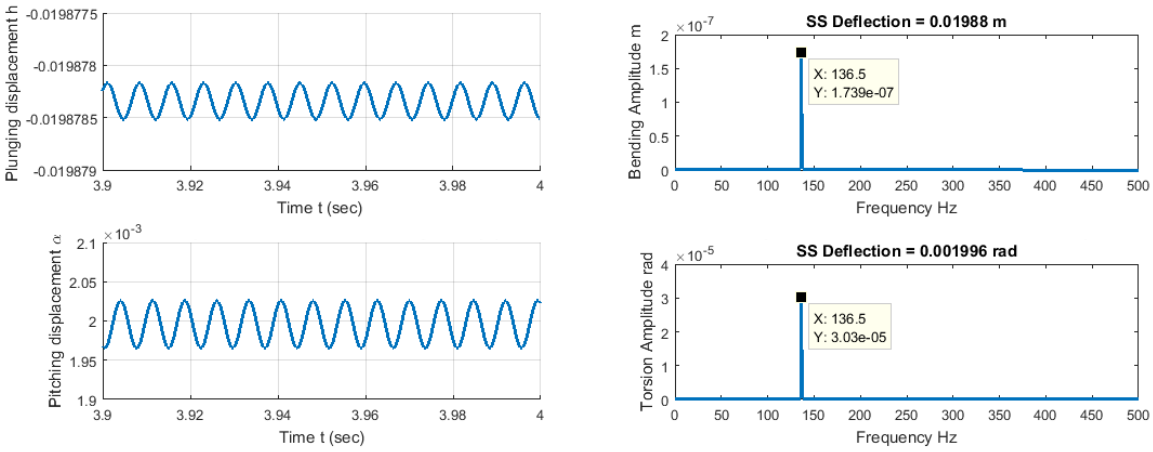

Figure 5 : Steady state analysis in time and frequency domains

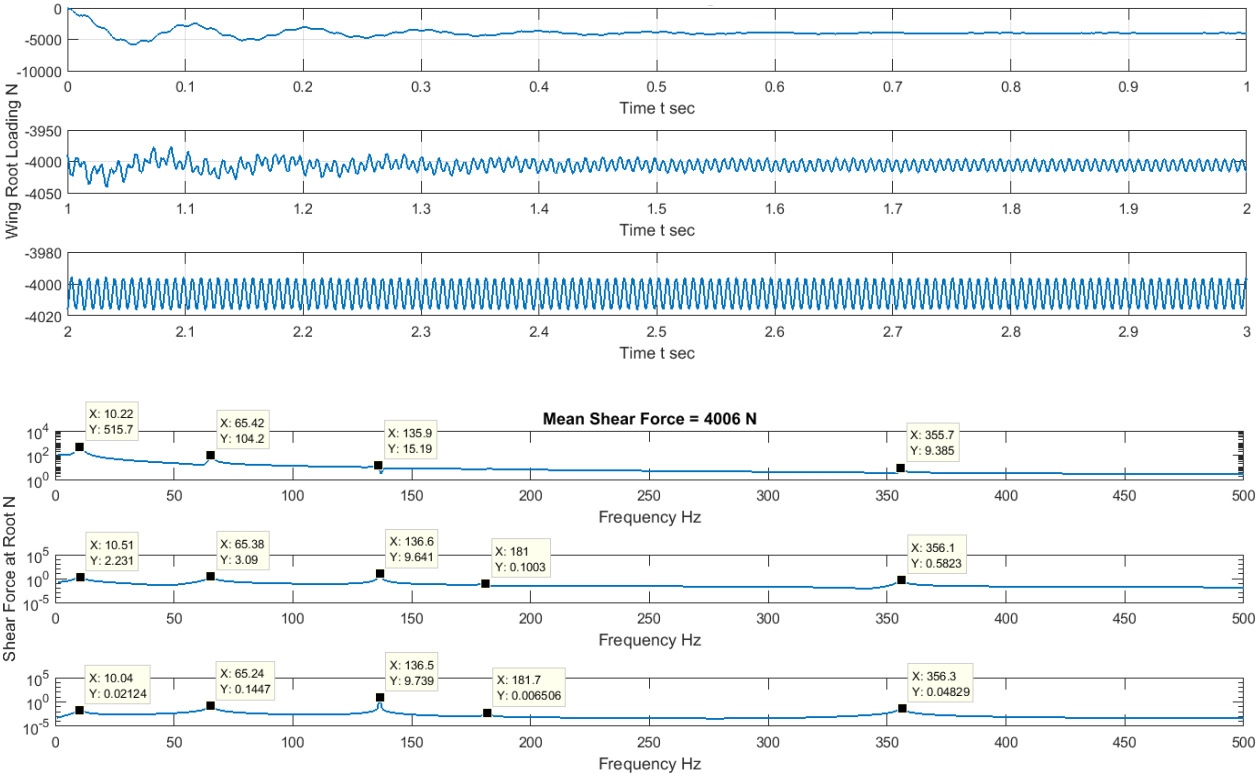

Figure 6: Shear force loading at wing root in time and frequency domains

Along with the wing displacements, also shear loads transferred from the wing to the fuselage at wing root are analysed in the study performed. Based on the full beam deflection history, the shear force generated on the wing root can be plotted as shown in Figure 6. As shear force is directly linked with third order derivatives of the bending behaviour, a similar pattern is observed with respect to the bending displacement response. To start with having the first mode governing the loading pattern, as it weakens, several higher frequencies can be observed. However all structural frequencies are damping down while propeller frequencies grows and contribute to steady state with a mean value of 4006 N. In Figure 6, both time-domain and frequency-domain responses are plotted to evaluate the magnitude and amplitude of the loads transferred to the fuselage.

3.4 Case Study Steady-State Analysis

In this subsection, a comparison between two different aerodynamic theories to model the propeller inflow as a sinusoidal gust is shown in this section. As discussed in Section 2.2, for a wing aerofoil travelling in sinusoidal gust, its aerodynamic loadings can also be characterised by Sears' model. Since it is developed in the frequency-domain, Sears' model provides the steady-state loads generated while the Küssner's theory, used in the previous section, allows to capture time-domain transient response.

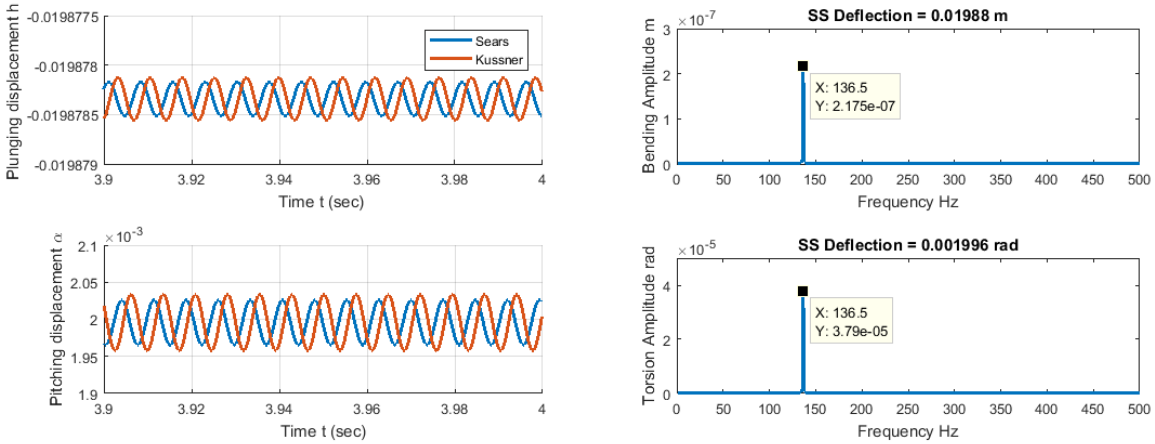

Figure 7: Sears' steady state analysis and comparison using Küssner's model

Taking into account five bending and one torsional modes with time step being 1/8 of the smallest period, Figure 7 presents the steady state behaviour given by Sears' model and its comparison with the Küssner's model. Similarity is shared between Sears' and Küssner's model for the relationship of structural behaviour and the sinusoidal localised gust (propeller inflow) contribution. Both methods gave the same steady state mean value and frequencies. Small differences lie in terms of the vibrating amplitude and phase. The difference in phase can be easily explained by the different gust implementation approach in the two methods assumed. While in the Sears' model the sinusoidal gust is applied everywhere chord-wise starting from t=0 seconds, for the Küssner's model the gust is considered travelling from the leading edge and through the chord. Therefore, phase lag difference are unavoidable. This makes Sears' model almost equivalent to the Küssner's one if steady-state behaviour needs to be analysed, but only the latter can accurately predict the system response if transient behaviour need to be captured.

4 CONCLUDING REMARKS AND FUTURE WORK

This paper presents a simplified and numerically efficient computational tool for time-domain aeroelastic analysis for the purpose to provide predictions accurate enough for the system aeroelastic response. It showed the structural formulations together with the analytical aerodynamic theory used, as well as aeroelastic response of a Eurocopter X3-like wing structure. Both the transient and steady-state responses are analysed utilising Küssner's and Sears' models. Steady-state results given by these two approaches are compared as well. Moreover, transient loading is characterised at the wing root. Overall, the aeroelastic tool is able to take account of motions in torsion and out-of-plane bending directions, wing pretwist angle, loading distribution along the span and any arbitrary gust in in-plane and out-of-plane directions.

The model can be further developed to take consideration of wing drag and forward thrust provided by the propeller. With respect to these loads, aeroelastic response in the in-plane bending can be disclosed. Being able to refine the structural model, an investigation towards the dynamic coupling between propeller-wing configuration considering nacelle attachment, gearbox and power transmission can be carried out to obtain a more detailed model able to provide also stability information about wing-propeller interaction.

REFERENCES

[1] H. Wagner, "Über die Entstehung des dynamischen Auftriebes von Tragflügeln," *Zeitschrift für angewandte Mathematik and Mechanik,* vol. 5, no. 1, pp. 17-35, 1925.

[2] T. von Karman and W. Sears, "Airfoil Theory for Non-Uniform Motion," *Journal of the Aeronautical Science,* vol. 5, no. 10, pp. 379-390, 1938.

[3] H. G. Küssner, "Zusammenfassender Bericht über den instationären Auftrieb von Flügeln," *Luftfahrtforschung,* vol. 13, no. 12, pp. 410-424, 1935.

[4] W. R. Sears and B. O. Sparks, "On the reaction of an elastic wing to vertical gusts," *Journal of the Aeronautical Sciences,* vol. 9, no. 2, pp. 64-67, 1941.

[5] R. T. Jones, "Operational treatment of the nonuniform-lift theory in airplane dynamics," NACA Technical Notes No.667, 1938.

[6] R. T. Jones, "The unsteady lift of a wing of finite aspect ratio," NACA Technical Notes No.681, 1940.

[7] M. H. Kargarnovin and A. Mamandi, "Aeroelastic response for pure plunging motion of a typical section due to sharp edged gust , using Jones approximation aerodynamics," *World Academy of Science, Engineering and Technology,* vol. 36, pp. 154-161, 2007.

[8] S. Shams, H. Haddadpour, M. H. Sadr Lahidjani and M. Kheiri, "An analytical method in computational aeroelasticity based on Wagner function," in *25th International Congress of the Aeronautical Science*, Hamburg, Germany, 2006.

[9] P. Marzocca, L. Librescu and G. Chiocchia, "Aeroelastic response of 2-D lifting surfaces to gust and arbitrary explosive loading signatures," *International Journal of Impact Engineering,* vol. 25, no. 1, pp. 41-65, 2001.

[10] G. Bernardini, E. Piccione, A. Anobile, J. Serafini and M. Gennaretti, "Optimal design and acoustic assessment of low-vibration rotor blades," *International Journal of Rotating Machinery,* vol. 2016, p. 17 pages, 2016.

[11] Y. Fung, An introduction to the theory of aeroelasticity, New York: Dover Publications Inc., 1955.

[12] A. Anobile, G. Bernardini, M. Gennaretti and C. Testa, "Synthesis of active twist controller for rotor blade–vortex interaction noise alleviation," *Journal of Aircraft,* vol. 53, no. 6, pp. 1865-1874, 2016.

[13] N. Newmark, "A method of computation for structural dynamics," *Journal of the Engineering Mechanics Division,* vol. 85, no. 3, pp. 67-94, 1959.

[14] R. Bisplinghoff, H. Ashley and R. Halfman, Aeroelasticity, Mineola, New York: Dover Publication Inc, 1983.

[15] J. Leishman, Principles of helicopter aerodyanmics, 2nd Edition, New York: Cambridge University Press, 2006.

[16] S. Shams, M. H. Sadr Lahidjani and H. Haddadpor, "Nonlinear aeroelastic response of slender wings based on Wagner function," *Thin-Walled Structures,* vol. 46, no. 11, pp. 1192-1203, 2008.